

Calibration-Free Gas Source Localization with Mobile Robots: Source Term Estimation Based on Concentration Measurement Ranking

Wanting Jin, Agatha Duranceau, İzzet Kagan Erünsal and Alcherio Martinoli

Abstract—Efficient Gas Source Localization (GSL) in real-world settings is crucial, especially in emergency scenarios. Mobile robots equipped with low-cost, in-situ gas sensors offer a safer alternative to human inspection in hazardous environments. Probabilistic algorithms enhance GSL efficiency with scattered gas measurements by comparing gas concentration measurements gathered by robots to physical dispersion models. However, accurately deriving gas concentrations from data acquired with low-cost sensors is challenging due to the nonlinear sensor response, environmental dependencies (e.g., humidity, temperature, and other gas influences), and robot motion. Mitigating these disturbance factors requires frequent sensor calibration in controlled environments, which is often impractical for real-world deployments. To overcome these issues, we propose a novel feature extraction algorithm that leverages the relative ranking of gas measurements within the dynamically accumulated dataset. By comparing the rank differences between gathered and modeled values, we estimate the probabilistic distribution of source locations across the entire environment. We validate our approach in high-fidelity simulations and physical experiments, demonstrating consistent localization accuracy with uncalibrated gas sensors. Compared to existing methods, our technique eliminates the need for gas sensor calibration, making it well-suited for real-world applications.

I. INTRODUCTION

Gas leak detection is critical for industrial safety, environmental protection, and public health [1]. Localizing the source of the leak is often time-sensitive, especially in emergency scenarios. However, measuring gas concentrations in large areas is time-consuming, as in-situ gas sensors provide only point measurements at specific locations and times. Consequently, efficiently estimating the source with only a limited number of measurements is of paramount importance. Probabilistic algorithms facilitate Gas Source Localization (GSL) with scattered gas measurements by incorporating knowledge of gas plume models [2]. They iteratively update the belief of each candidate source position by assessing the alignment between the **measured gas concentrations** derived from the sensor readings and the **estimated gas concentrations** derived from gas plume models. However, real-world GSL is challenging because of the limited faithfulness of plume models and reliability of concentration measurements. In this work, we propose

The authors are with the Distributed Intelligent Systems and Algorithms Laboratory, School of Architecture, Civil and Environmental Engineering, École Polytechnique Fédérale de Lausanne (EPFL), 1015 Lausanne, Switzerland. This work is funded by the Swiss National Science Foundation under grants 200020_175809 and 10.001.747. Additional information about the research can be found here: <https://disal.epfl.ch/research/gassensingstructure/>

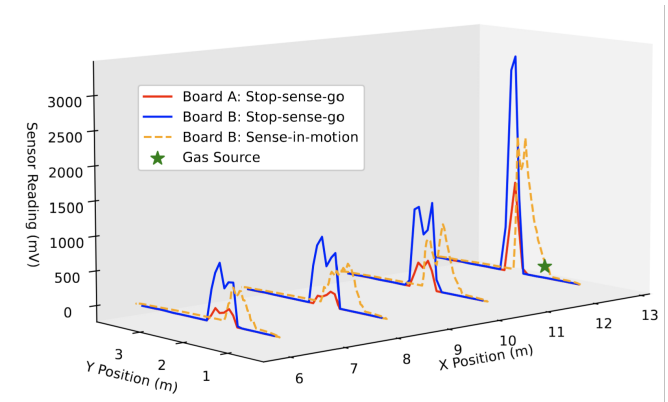


Fig. 1: Gas measurements collected using different sensor boards (A and B) and gas sampling strategies (*stop-sense-go* and *sense-in-motion*). The difference in sensor responses highlights the impact of both sensor properties and robot motion on gas measurement consistency.

addressing the **model-to-measurement gap** with a gas feature that reduces dependency on precise plume models while effectively utilizing raw sensor readings to retain information for probabilistic GSL algorithms.

Given the complexity of conducting GSL experiments in the real world, many existing works are performed solely in simulation [3]–[7]. However, two critical challenges are often overlooked, which limits the transfer of these methods to real-world applications: (i) complex environmental layouts with obstacles, and (ii) the slow, nonlinear response of physical gas sensors to changes in gas concentration. In [3] [4], the environment is assumed to be obstacle-free, and therefore the gas dispersion can be modeled analytically under a steady regime assumption. In realistic settings, however, obstacles can significantly influence the gas dispersion pattern, making analytical solutions infeasible. To address challenge (i), one promising approach proposed in our previous work is to use a Data-Driven Plume Model (DDPM) as a surrogate gas plume model for built environments [8]. DDPM is a learning-based method that predicts the gas concentration distribution given a hypothesized source location and environmental layout. Regarding challenge (ii), in [5]–[7] gas sensor outputs are treated as accurate concentration measurements perturbed only by white noise. In practice, however, physical gas sensors such as Metal Oxide (MOX) sensors, depend on direct exposure and chemical interaction with the target gas, and therefore exhibit slow and nonlinear response to concentration changes. In addition, these sensors usually have slow response and recovery dynamics, which can lead to

spatial misalignment when measurements are collected while the robot is moving.

To illustrate this, Fig. 1 highlights the impact of sensor properties and robot motion on gas measurements. The solid red and blue lines show outputs from two MiCS-5521 MOX sensor boards in a *stop-sense-go* mode, where the robot pauses at each sampling point. The orange dashed line shows readings from the same sensor board as the blue line, but in a *sense-in-motion* mode, where measurements are taken continuously during motion. The difference across these results highlights two key effects: (1) individual sensors can produce different responses under identical conditions, and (2) sampling in motion reduces signal magnitudes and shifts peak position due to shorter gas contact time and slow sensor dynamics [9] [10]. Therefore, a direct comparison between estimated gas concentrations by DDPM and measured concentrations is nontrivial. While the absolute values of sensor readings vary across conditions, the overall evolution remains similar. These observations motivate us to consider the design of alternative features that are robust to sensor variability and motion-induced artifacts.

A. Related Work

Various gas features have been explored for GSL tasks, with the most commonly used ones being absolute gas concentration values and gas hit events. Several studies use concentration values directly, assuming a linear relationship between sensor output and actual concentration, modulated by a scaling factor [11]–[14]. This model is only valid at low concentrations, where sensor nonlinearity is negligible [15]. To address this point, [16] approximates the nonlinear response between the output voltage reading with actual gas concentration. However, this nonlinearity varies with gas type, manufacturing variability, environmental conditions (e.g., humidity, temperature, interfering gases), and sensor aging [17]. As a result, each sensor must be calibrated with known concentrations of gas mixture in controlled conditions with a dedicated gas chamber to ensure accurate concentration approximation [18] [19]. Frequent calibration is required as the aforementioned environmental variations are uncontrollable, which makes it impractical in real-world settings. Gas hit events, binary indicators of gas presence or absence, which can be triggered by fixed [20] [21] or adaptive [22] thresholds, offer an alternative feature. Compared to gas concentration values, gas hit events are more robust to sensor noise and drift. However, the binarization discards the gradient information from the measurements, and their accuracy depends heavily on the threshold selection.

B. Problem Statement

The objective of this work is to localize the 2D position of a single gas leak source in indoor environments with obstacles. We assume the leakage time is long enough for the plume to reach a steady state. The environmental layout and the inlet wind speed are assumed to be known. The input of the system are the gas concentration measurements gathered by a low-cost MOX sensor embedded on a mobile

robot. At each iteration, the algorithm outputs a belief map indicating the likelihood of the source being in each part of the environment. The algorithm is terminated when the belief map converges or the maximum number of iterations is reached, and the final output is the estimated source location.

C. Contribution

In this work, we address the problem of localizing a single gas leak source with a ground robot equipped with a MOX gas sensor. To eliminate the need for tedious sensor calibration while preserving spatial gas intensity information, we introduce a novel rank-based gas feature that incorporates a probabilistic GSL algorithm. This method compares the relative ranking sequence of measured and estimated gas concentrations within their respective datasets, capturing structural similarity under the assumption of a nonlinear but monotonic relationship. By focusing on relative magnitude evolution rather than absolute values, this approach enables direct deployment on mobile robots endowed with uncalibrated MOX sensors. More concretely, this paper presents the following contributions.

- **MOX sensor simulation:** a faithful model that captures the nonlinear response and slow dynamics of a MOX sensor, integrated into the simulation pipeline.
- **Rank-based gas feature:** a novel gas feature that encodes the relative rank of each concentration measurement within the dataset.
- **STE framework integration:** the integration of the proposed feature, along with three existing features, into a probabilistic Source Term Estimation (STE) framework [23], enabling comprehensive benchmarking of the gas feature selection.
- **Experimental validation:** a comprehensive evaluation of the resulting algorithmic pipeline through high-fidelity simulations and real-world experiments with different MOX sensors.

The outline of the paper is as follows: Section II presents the proposed gas feature together with three alternative variants typically leveraged in the literature and their integration into a STE framework. Simulation and physical experiment results are detailed in Sections III and IV, respectively. Finally, Section V provides a discussion of the findings and future research directions.

II. METHODOLOGY

The STE algorithm is designed to estimate key parameters influencing the gas dispersion process, such as the source position, based on an inverse modeling approach [23].

Overview of the STE: An overview of our STE algorithm with gas feature extraction is shown in Fig. 2. The environment is discretized into a grid, and each cell's probability of containing the source is iteratively evaluated. At each iteration, a steady-state gas dispersion model simulates plumes from every candidate cell and estimates the expected concentrations at the robot's sampling positions. The alignment between gas features extracted from the *Gas Sensing Module* and those from the *Gas Dispersion Model*

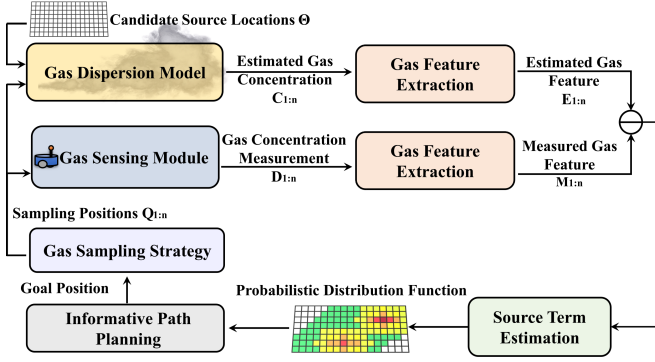


Fig. 2: STE algorithm flowchart

updates the probability of each cell containing the source. The resulting Probability Distribution Function (PDF) over source positions guides *Informative Path Planning* algorithm, enabling more efficient data collection and accelerating estimation convergence. A new iteration begins once the robot reaches its goal and acquires a new batch of gas measurements.

Let Θ be a random variable representing the unknown source location. The environment is discretized into N grid cells, with candidate source locations represented by $\{\Theta_1, \Theta_2, \dots, \Theta_N\}$, with Θ_j denotes the center coordinates of cell j . For each iteration, let $D_{1:n} = \{d_1, \dots, d_n\}$ represent all the gas measurements gathered by the robots across sampling locations denoted by $Q_{1:n} = \{q_1, \dots, q_n\}$. For each possible source location Θ_j , the gas dispersion model simulates the gas plume with the gas source located at Θ_j and derives the estimated gas concentrations represented by $C_{1:n} = \{c_1, \dots, c_n\}$ across the same set of sampling positions $Q_{1:n}$. The gas features extracted from the measured gas concentration $D_{1:n}$ are denoted by $M_{1:n} = \{m_1, \dots, m_n\}$, while those extracted from the estimated gas concentration $C_{1:n}$ are represented by $E_{1:n} = \{e_1, \dots, e_n\}$. Each component of the STE algorithm is detailed in the following sections.

A. Gas Dispersion Model

To incorporate the physical knowledge into the estimation process, a gas plume (dispersion) model is essential for predicting expected gas concentrations given a hypothesized source location Θ_j . To extend the applicability of STE to typical built environments, where closed-form model such as the Pseudo-Gaussian plume model [24] can not be used, a DDPM was proposed in [8] as a surrogate gas plume model. This approach leverages a Convolutional Neural Network (CNN) trained with gas dispersion maps under various environments with different obstacle configurations and source locations. The DDPM takes the obstacle configuration and hypothesized source location Θ_j as input and outputs the corresponding estimated gas concentration values $C_{1:n}$. The same DDPM approach is leveraged in this work; for more information about its structure and training process, please refer to [8].

B. Gas Sensing Module in Simulation

The robot samples the gas concentration at 10 Hz with an embedded MOX sensor. To have a faithful representation of the physical MOX sensor, three key characteristics are incorporated into the high-fidelity simulator. The simulated sensor model and the sensor data processing flowchart is shown in Fig. 3.

1) *Nominal sensor model*: The MOX sensor comprises a heated metal oxide surface whose electrical resistance (R_s) changes in response to the interaction with oxidizing gases. A simple voltage divider circuit is used to measure R_s , incorporating a supply voltage V_T and a load resistor R_L . The sensor output V_{out} is the voltage measured across R_L , from which R_s can be computed using the voltage divider equation. According to the sensor datasheet, the logarithm of the ratio between R_s and its baseline resistance in clean air R_0 exhibits a linear relationship with the logarithm of the gas concentration g_{con} .

$$\log(g_{con}) = k * \log\left(\frac{R_s}{R_0}\right) + b \quad (1)$$

The parameters k and b define the nonlinear sensor response and depend on gas type and sensor sensitivity. Due to manufacturing variations, each sensor may have different R_0 and sensitivity values. Additionally, k, b, R_0 are further influenced by environmental factors such as humidity and temperature. Combining these elements, the actual gas concentration g_{con} can be approximated from the sensor output V_{out} using:

$$g_{con} = \mathcal{F}(V_{out}, [k, b, R_0]) = 10^b * \left(\frac{R_L V_T - R_L V_{out}}{R_0 V_{out}}\right)^k \quad (2)$$

The sensor model is nonlinear, and the parameters k, b and R_0 must be obtained through calibration. Let v_i and d_i represent sensor output, which is voltage in our case, and gas concentration measurement at the i th sampling position, respectively. To calculate d_i :

- For calibrated sensors, $d_i = \mathcal{F}(v_i, [k, b, R_0])$, where $\mathcal{F}(\circ)$ is the calibration function in Eq. 2. In this case, gas concentration measurement corresponds to the approximate gas concentration.
- For an uncalibrated sensor, no transformation is applied, and the gas concentration measurement is obtained by directly taking the value of the sensor output $d_i = v_i$.

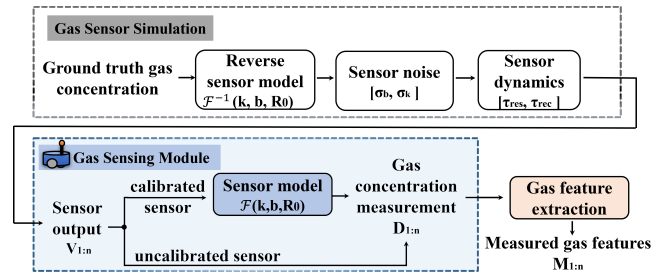


Fig. 3: Data flow for the gas sensor simulation and gas sensing module

2) *Sensor noise*: The additive sensor noise σ_s is modeled as the sum of two components: background noise σ_b which has a fixed value, and gas intermittency noise σ_k , which is simulated as a proportional variation of the sensor output.

$$\sigma_s = \sigma_b + \sigma_k * |v_i| \quad (3)$$

with σ_b and σ_k are obtained via estimation from physical sensor outputs.

3) *Sensor dynamics*: MOX sensors exhibit slow dynamics, requiring a certain amount of time to transition from a baseline reading to a stabilized value when exposed to gas, and vice versa when exposed to clean air. Response and recovery phases of a MOX sensor are modeled as first-order systems, as described in [25] [26]. The parameters of the simulated MOX sensor are calibrated to match the actual deployed sensor (MiCS-5521), with a response time τ_{res} and recovery time τ_{rec} of 2.04 s and 4.57 s, respectively.

C. Gas Features

Gas features are used to evaluate the correlation between measured and estimated gas concentration. In the following, we present a novel gas feature based on concentration ranking, together with three existing ones typically adopted in previous studies.

1) *Gas measurement value*: The measured and estimated gas concentration values are directly adopted as gas features, which are defined as $m_i = d_i$ and $e_i = c_i$.

2) *Gas measurement hit*: A gas measurement hit is defined as a binary value determined by a threshold. It is formulated as $m_i = 1$ if $d_i > d_{thres}$ and $m_i = 0$ otherwise, where d_{thres} is the threshold for measured gas hits. The same formulation is applied to the estimated gas hits using a corresponding threshold c_{thres} .

This threshold can be either fixed or adaptive. We refer to the feature as *fixed gas hit*, when a manually selected threshold is applied and remains constant throughout the experiments. In the case of an adaptive threshold, which we refer to as *adaptive gas hit*, we adopt the formulation proposed in [22]. The threshold $\bar{d}_{thres,i}$ is dynamically updated using a moving window average:

$$\bar{d}_{thres,i} = \begin{cases} \lambda \bar{d}_{thres,i-1} + (1 - \lambda) d_i & \text{if } i \geq 2, \\ d_1 & \text{if } i = 1, \end{cases} \quad (4)$$

The parameter $\lambda \in [0, 1)$ controls the smoothing factor. This feature enables detecting the gas hits at the rising edges of the smoothed gas concentration measurements. The same formulation is applied to the estimated gas hits, with $\bar{c}_{thres,i}$ computed from $C_{1:n}$. We choose λ as 0.7 based on an exhaustive search, selecting the value that yields the best performance.

3) *Gas measurement rank*: We propose using the relative measurement rank as the gas feature to mitigate the dependency on accurate gas concentration measurements (as assumed by the *gas measurement value* feature) and avoid the loss of relative magnitude variation (as resulting from the *gas measurement hit* feature). To this purpose, we

compare the relative rankings of measured and estimated gas concentrations across all sampling points. Specifically, for a gas concentration measurement d_i and its corresponding estimate c_i at the same location, we compute their ranks within the respective datasets $D_{1:n}$ and $C_{1:n}$. This ranking-based approach captures the evolution of gas concentration patterns and assesses the alignment between measured and estimated values without relying on their absolute magnitudes. Because of this characteristic, it does not assume any specific functional relationship between measured and estimated gas concentration. It remain valid as long as a positive monotonic relationship is maintained, which means $D_{1:n}$ is considered to be aligned with $C_{1:n}$ as long as a higher measured gas concentration corresponds to a higher estimated gas concentration. To formalize this, we use the Empirical Distribution Function (EDF), which assigns a normalized rank to each measurement within the dataset without specific assumptions about the underlying data distribution. The EDF-based gas feature is defined as:

$$m_i = \frac{1}{n} \sum_{j=1}^n \mathbf{1}_{d_j \leq d_i} \quad (5)$$

where $\mathbf{1}_A$ is the indicator of event A, which returns 1 if event A is true and 0 otherwise. Thus, m_i represents the proportion of measurements in $D_{1:n}$ that are less than or equal to d_i , yielding a value in the range $[0, 1]$. This formulation transforms gas measurements into scale-invariant, rank-normalized features. The same procedure is applied to the estimated gas concentrations $C_{1:n}$ to compute the EDF-based feature e_i . Unlike the other three features, the EDF values m_i and e_i are dynamically updated at each iteration as new measurements are collected over successive iterations. Regarding the computational complexity, we do not need to resort the entire dataset at every iteration. Suppose L measurements have been collected up to the previous iteration and their values are maintained in sorted order, and suppose P new measurements are acquired in the current iteration. We first sort the P new measurements, and then merge the two ranked lists. Therefore, the per-iteration computational complexity is $O(L + P \log P)$ (with $L + P = n$). In practice, when $L \gg P$, the update is dominated by the linear-time merge step.

D. Estimation Process

For each candidate source location Θ_j , the likelihood $p(D_{1:n}|\Theta_j)$ is calculated through the similarity across each m_i and e_i at the i th sampling point. Here, σ_M and σ_E represent the standard deviations of the measurement and model estimation errors, respectively.

$$p(D_{1:n}|\Theta_j) \propto \exp\left(-\frac{1}{2} \sum_{i=1}^n \frac{n}{n+1} \frac{(e_i(\Theta_j) - m_i)^2}{\sigma_E^2 + \sigma_M^2}\right) \quad (6)$$

Compared to the conventional likelihood function used in many existing works [27] [12], we introduce in this work an additional $\frac{n}{n+1}$ term that accounts for the number of measurements. This adjustment mitigates the risk of

premature convergence when measurements are sparse and scattered. Bayesian inference is used to update the posterior PDF $p(\Theta | D_{1:n})$, representing the probability distribution of the source position across Θ . We consider the prior $p(\Theta)$ to be a uniform distribution within the estimation area and assume a zero value inside the obstacles and boundary areas.

E. Gas Sampling Strategy

The *stop-sense-go* strategy is commonly used in the literature due to gas plume intermittency and the slow sensor response. However, it reduces efficiency by prolonging the measurement process and discarding data collected during motion. In previous work [28], the feasibility of employing a *sense-in-motion* strategy is studied, where measurements $D_{1:n}$ are continuously taken on the way points $Q_{1:n}$ while the robot is moving. Despite increased noise in gas measurements, the increased measurement density compensates for reduced quality, resulting in a more efficient and robust sensing system. Therefore, we adopt the *sense-in-motion* strategy in this work as well.

F. Informative Path Planning

The posterior PDF is used to calculate the information gain of the robot motion. Building on the sense-in-motion strategy, we adopt in this work a previously proposed informative path planning method called belief-clustering [28], which considers the information gained along the entire trajectory.

G. Termination Condition

The algorithm terminates when the entropy of the posterior PDF $p(\Theta | D_{1:n})$ drops below a predefined threshold and the set of candidate cells with high posterior probability is confined to a small spatial region, or when the maximum number of iterations is reached. Upon termination, the grid cell with the highest posterior probability is taken as the estimated source location. We set the maximum number of iterations to 30 in simulation and 40 in physical experiments. The higher limit in physical experiments accounts for the greater intermittency of real plumes, which makes gas measurements less reliable and slows convergence.

III. SIMULATION RESULTS

Simulations are conducted using the high-fidelity robotic simulator Webots [29], with a dedicated gas dispersion plugin [30]. The testing environment includes two rectangular obstacles positioned centrally to create significant airflow disturbances, thereby influencing the gas dispersion dynamics, which is a typical environmental setup aligned with the work reported in [28]. The simulation setup is shown in Fig. 4. The performance of each feature is evaluated based on GSL accuracy and efficiency. GSL accuracy is determined by the source localization error, measured as the Euclidean distance between the estimated and true source positions. At each iteration, the robot updates its belief about the source position and selects the next goal position. To evaluate the GSL efficiency, the number of iterations required for the STE to converge is analyzed. Each experimental trial consists of

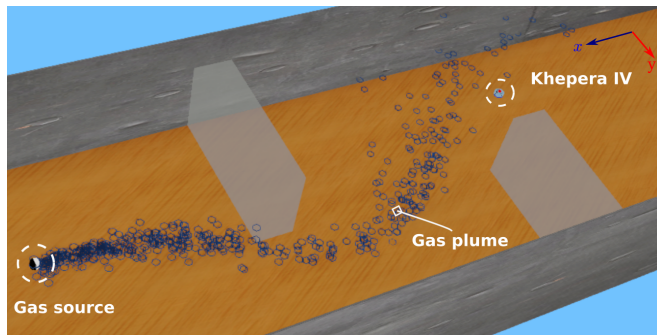


Fig. 4: A screenshot from the Webots simulator displaying the environment with obstacles, gas plume and robot.

ten runs with randomized source locations and robot starting positions. Out of brevity, we will use the terms “*gas value*”, “*gas rank*”, “*fixed gas hit*” and “*adaptive gas hit*” to refer to the gas features in the following text.

The performance of different gas features is evaluated using raw sensor voltage outputs from uncalibrated MOX sensors. For comparison, we also report results obtained with calibrated sensors. In the uncalibrated setting, we consider two different samples of MOX sensors, referred to as *Sensor I* and *Sensor II*, which differ in their base resistances R_0 and thus capture different levels of nonlinearity in the relationship between sensor output and actual gas concentration. We simulate the output voltage reading of uncalibrated MOX sensors through reverse sensor modeling, as demonstrated in Fig. 3. Specifically, two values of R_0 are considered: $100\text{ k}\Omega$ and $1500\text{ k}\Omega$, for *Sensor I* and *II* respectively, corresponding to the minimum and maximum factory variations specified in the sensor datasheet. The parameters $k = -1.58$ and $b = 0.17$ are fixed based on datasheet calibration for ethanol detection under test conditions of $23 \pm 5^\circ\text{C}$ and $50 \pm 10\%$ RH. In the calibrated setting, we use the same value of $[k, b, R_0]$ used for the reverse sensor modeling to calculate the calibrated gas concentration measurements.

The results shown in Fig. 5 indicate that all features achieve similar localization accuracy with the calibrated gas sensor. The *gas value* feature converges faster by retaining most information from gas measurements and directly

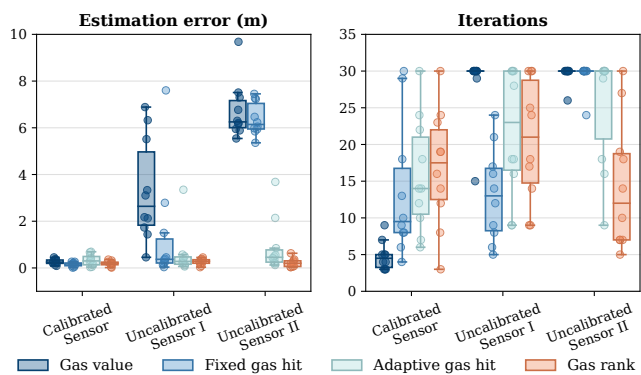


Fig. 5: Performance comparison of the four different gas features with different gas sensors in simulation.

leverages magnitude differences in the likelihood function. When an approximated gas concentration closely matches the expected value near the gas source, rapid convergence occurs. In contrast, other features converge more slowly since the information is more abstract. However, the *gas value* feature lacks robustness with uncalibrated gas sensors, as gas concentration measurements, corresponding to raw sensor outputs in this case, no longer reflect actual gas concentrations. A similar limitation occurs with the *fixed gas hit* feature, where the manually selected threshold fails to adapt to sensor models. In contrast, the *adaptive gas hit* and *gas rank* features remain consistent across different sensor models. They rely solely on a positive monotonic relationship between sensor outputs and gas concentrations, which preserves the rising edge and overall ranking of values despite nonlinearity. Here, we demonstrate the robustness of the proposed gas features under different sensor models by varying R_0 . In principle, the same features can also generalize across different target gases, which would induce different sensor response curves (captured by different values of k and b). This is because these features only require a positive monotonic relationship between sensor output and gas concentration, which is preserved for arbitrary R_0 , k and b .

Among these features, *gas rank* outperforms *adaptive gas hit* in localization accuracy and convergence efficiency. This is because sensor noise can lead to incorrect gas hit detections, and since *adaptive gas hit* captures only local trends, it is more sensitive to these fluctuations. In contrast, *gas rank* considers the entire data distribution, mitigating the impact of local noise and enhancing robustness. Furthermore, compared to *adaptive gas hit*, it requires no extra hyperparameter tuning (λ in Eq. 4).

IV. PHYSICAL EXPERIMENTS RESULTS

This section evaluates the *gas value* (baseline) and *gas rank* features employed with the STE algorithm for physical GSL experiments.

A. Experimental Setup

The experiments were carried out within our wind tunnel facility, ensuring consistent testing conditions across multiple runs. The wind tunnel has a volume of $18 \times 4 \times 1.9$ m and is equipped with a Motion Capture System (MCS) for accurate robot localization. The wind speed was maintained at 0.75 m/s throughout all experiments. The gas dispersion was generated using an electric pump vaporizing ethanol. We configured the wind tunnel with the same obstacle layout as in simulation, as shown in Fig. 6. A Khepera IV robot, equipped with a gas sensing module featuring a MiCS-5521 MOX sensor sampled at 10 Hz, was used as the mobile robotic platform. The robot's maximum speed was set to 0.27 m/s. The STE algorithm was executed on a laptop with an Intel Core i7-12700H processor. After each iteration, a new goal position was sent to the robot. The robot navigated to the goal point, collected gas samples continuously during

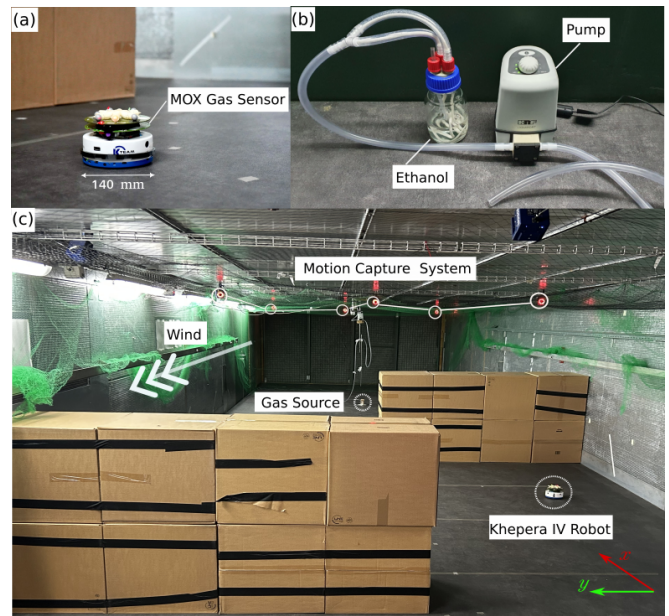


Fig. 6: a) A Khepera IV robot equipped with the gas sensing module. b) Gas source. c) Experimental arena in the wind tunnel.

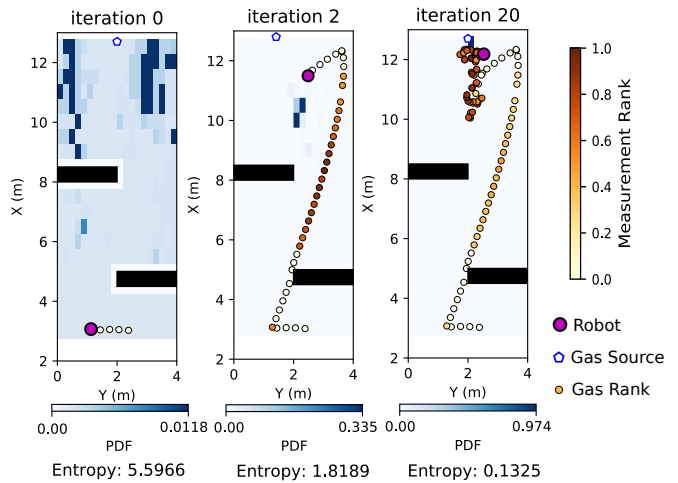


Fig. 7: Illustration of the estimation process of one experimental run.

motion, and transmitted them back to the laptop. The robot communicated with the laptop over high-speed WiFi.

Given the effort required to conduct physical experiments for GSL tasks, we choose the *gas value* feature as the baseline, as it is the canonical choice in most state-of-the-art STE methods [7] [28]. To thoroughly evaluate the robustness of the *gas rank* feature, we use two uncalibrated gas sensor boards (A and B) with distinct characteristics, as shown in Fig. 1, and varying source locations. For each gas feature, fifteen experiments were conducted, with the gas source fixed along the x -axis, the y -axis varied across $\{1, 2, 3\}$ meters to ensure broad spatial coverage.

B. Results and Discussion

An illustration of the estimation process of one experimental run using the *gas rank* feature is shown in Fig. 7. The

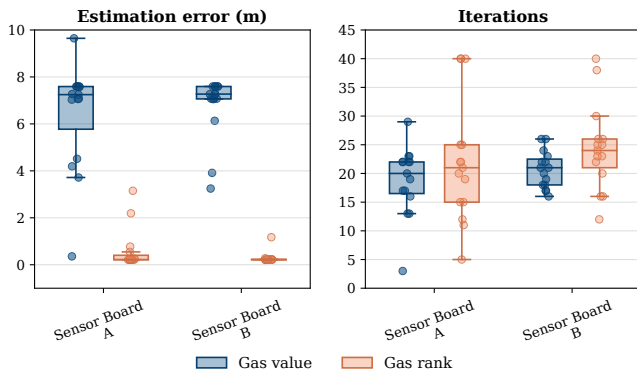


Fig. 8: Physical experiments with two sensor boards.

background color map in each subplot represents the current PDF over potential source locations. The circles along the robot’s trajectory represent gas measurements collected during motion, with their color indicating the EDF value, which is the rank-based gas feature. Over each iteration, the robot incrementally augments its dataset by exploring the environment. As new measurements are gathered, the relative EDF values are updated accordingly. Initially, the source belief is broadly distributed across the environment (left), but as more measurements are collected, the distribution becomes increasingly concentrated (middle), ultimately converging near the true source location (right).

The results in Fig. 8 show that the *gas rank* feature successfully localizes the gas source with different gas sensors, without requiring sensor calibration and any parameter tuning. It performs consistently across sensor variations and source positions. In contrast, *gas value*, which is typically used in the literature, fails to converge to the true source location with uncalibrated sensors. These findings align with the results observed in simulations. However, a higher localization error with some outliers is observed in real experiments compared to simulation. This discrepancy may be attributed to the increased intermittency due to turbulence of the gas plume and the accumulation of the gas in some region in the physical world, a phenomenon not faithfully reproduced in simulation.

V. CONCLUSION AND OUTLOOK

In this paper, we address the challenge of GSL using low-cost MOX gas sensors, which exhibit a nonlinear yet positive monotonic relationship between sensor outputs and actual gas concentrations. Due to their sensitivity to environmental parameters (e.g., temperature, humidity, other interfering gases), achieving and maintaining accurate sensor calibration is not practical. To overcome this limitation, we propose a novel *gas rank* feature. It ranks measured gas concentration and compares the ranks to those of estimated concentrations derived from a gas plume model. This approach eliminates the need for sensor calibration to approximate the actual gas concentration values, as it only considers the relative shape of the data distribution across sampling locations. As a consequence, the proposed feature is robust to differences

in magnitude and nonlinear mapping between sensor outputs and actual gas concentrations.

The proposed method is evaluated in both simulation and physical experiments and compared with three existing gas features: *gas value*, *fixed gas hit*, and *adaptive gas hit*. Results show that both the *adaptive gas hit* and *gas rank* features demonstrate superior robustness to uncalibrated sensors. Between these two robust features, the *gas rank* outperforms *adaptive gas hit* in term of localization accuracy and convergence speed. Additionally, unlike other features, *gas rank* does not require additional parameter tuning, such as the threshold for *fixed gas hit* or the smoothing parameter (λ) for *adaptive gas hit*.

Given the fact that the only assumption to use this feature is the positive monotonic relationship between sensor outputs and actual concentration, this approach is adaptable to different sensor types and source estimation tasks. Moreover, as it depends solely on the ranking sequence of measurement values within respective datasets, it opens the door for multi-robot systems with heterogeneous gas sensors. In such settings, each robot can estimate source parameters based on its own gas concentration measurements and share probabilistic estimates with other robots without requiring cross-calibration of sensors.

Further improvements could enhance the convergence speed and reduce the outliers of the STE algorithm leveraging our novel *gas rank* feature. Currently, only the rank of each measurement value is considered, but incorporating the slope (steepness) of the EDF function could provide additional information about how rapidly gas measurements changes spatially. This could lead to faster convergence and more robust localization of the source.

REFERENCES

- [1] T. Jing, Q. Meng, and H. Ishida, “Recent Progress and Trend of Robot Odor Source Localization,” *IEEJ Transactions on Electrical and Electronic Engineering*, vol. 16, no. 7, pp. 938–953, July 2021, number: 7.
- [2] A. Keats, E. Yee, and F.-S. Lien, “Bayesian inference for source determination with applications to a complex urban environment,” *Atmospheric Environment*, vol. 41, no. 3, pp. 465–479, Jan. 2007.
- [3] M. Hutchinson, H. Oh, and W.-H. Chen, “Adaptive Bayesian Sensor Motion Planning for Hazardous Source Term Reconstruction,” *IFAC-PapersOnLine*, vol. 50, no. 1, pp. 2812–2817, July 2017.
- [4] V. P. Ruiz, P. Hinsen, T. Wiedemann, D. Shutin, and C. Christof, “Gas Source Localization Using Physics-Guided Neural Networks,” in *2024 IEEE International Symposium on Olfaction and Electronic Nose*, May 2024, pp. 1–3.
- [5] R. V. Nanavati, M. J. Coombes, and C. Liu, “Distributed multi-robot source term estimation with coverage control and information theoretic based coordination,” *Information Fusion*, vol. 111, p. 102503, Nov. 2024.
- [6] S. An, M. Park, and H. Oh, “Receding-horizon RRT-Infotaxis for autonomous source search in urban environments,” *Aerospace Science and Technology*, vol. 120, p. 107276, Jan. 2022.
- [7] Y. Shi, M. Wen, Q. Zhang, W. Zhang, C. Liu, and W. Liu, “Autonomous goal detection and cessation in reinforcement learning: a case study on source term estimation,” in *Proceedings of the Thirty-Ninth AAAI Conference on Artificial Intelligence*, vol. 39, 2025, pp. 738–745.
- [8] W. Jin, F. Rahbar, C. Ercolani, and A. Martinoli, “Towards Efficient Gas Leak Detection in Built Environments: Data-Driven Plume Modeling for Gas Sensing Robots,” in *IEEE International Conference on Robotics and Automation*, May 2023, pp. 7749–7755.

- [9] W. Jin, E. Droz, and A. Martinoli, "Design and Evaluation of Modular Gas and Wind Sensing Nodes for Static and Mobile Deployments," in *IEEE/ASME International Conference on Advanced Intelligent Mechatronics*, July 2024, pp. 560–567.
- [10] K. C. Hoffman, J. M. Anderson, and K. K. Leang, "Rapid Airborne Gas-Plume Mapping and Source Localization With Feedforward Gas-Sensor Dynamics Compensation," *ASME Letters in Dynamic Systems and Control*, vol. 4, no. 4, p. 041002, Oct. 2024.
- [11] F. Rahbar, A. Marjovi, and A. Martinoli, "Design and Performance Evaluation of an Algorithm Based on Source Term Estimation for Odor Source Localization," *Sensors*, vol. 19, no. 3, p. 656, Feb. 2019.
- [12] M. Hutchinson, C. Liu, and W.-H. Chen, "Information-based search for an atmospheric release using a mobile robot: Algorithm and experiments," *IEEE Transactions on Control Systems Technology*, vol. 27, no. 6, pp. 2388–2402, 2018.
- [13] H. Zhu, Y. Wang, C. Du, Q. Zhang, and W. Wang, "A novel odor source localization system based on particle filtering and information entropy," *Robotics and Autonomous Systems*, vol. 132, p. 103619, Oct. 2020.
- [14] K. Jakkala and S. Akella, "Probabilistic Gas Leak Rate Estimation Using Submodular Function Maximization With Routing Constraints," *IEEE Robotics and Automation Letters*, vol. 7, no. 2, pp. 5230–5237, Apr. 2022.
- [15] C. Wang, L. Yin, L. Zhang, D. Xiang, and R. Gao, "Metal Oxide Gas Sensors: Sensitivity and Influencing Factors," *Sensors*, vol. 10, no. 3, pp. 2088–2106, Mar. 2010.
- [16] T. Wiedemann, D. Shutin, and A. J. Lilienthal, "Model-based gas source localization strategy for a cooperative multi-robot system—A probabilistic approach and experimental validation incorporating physical knowledge and model uncertainties," *Robotics and Autonomous Systems*, vol. 118, pp. 66–79, Aug. 2019.
- [17] N. Dennler, S. Rastogi, J. Fonollosa, A. Van Schaik, and M. Schmücker, "Drift in a popular metal oxide sensor dataset reveals limitations for gas classification benchmarks," *Sensors and Actuators B: Chemical*, vol. 361, p. 131668, June 2022.
- [18] P. P. Neumann, P. Hirschberger, Z. Baurzhan, C. Tiebe, M. Hofmann, D. Hullmann, and M. Bartholmai, "Indoor Air Quality Monitoring using flying Nanobots: Design and Experimental Study," in *IEEE International Symposium on Olfaction and Electronic Nose*, May 2019, pp. 1–3.
- [19] M. Turdúev, G. Cabrita, M. Kırtay, V. Gazi, and L. Marques, "Experimental studies on chemical concentration map building by a multi-robot system using bio-inspired algorithms," *Autonomous Agents and Multi-Agent Systems*, vol. 28, no. 1, pp. 72–100, Jan. 2014.
- [20] P. Ojeda, J. Monroy, and J. González-Jiménez, "Information-Driven Gas Source Localization Exploiting Gas and Wind Local Measurements for Autonomous Mobile Robots," *IEEE Robotics and Automation Letters*, vol. 6, no. 2, pp. 1320–1326, Apr. 2021.
- [21] T. Wiedemann, M. Schaab, J. M. Gomez, D. Shutin, M. Scheibe, and A. J. Lilienthal, "Gas Source Localization Based on Binary Sensing with a UAV," in *IEEE International Symposium on Olfaction and Electronic Nose*, May 2022, pp. 1–3.
- [22] J.-G. Li, Q.-H. Meng, Y. Wang, and M. Zeng, "Odor source localization using a mobile robot in outdoor airflow environments with a particle filter algorithm," *Autonomous Robots*, vol. 30, no. 3, pp. 281–292, Apr. 2011.
- [23] M. Hutchinson, H. Oh, and W.-H. Chen, "A review of source term estimation methods for atmospheric dispersion events using static or mobile sensors," *Information Fusion*, vol. 36, pp. 130–148, July 2017.
- [24] N. Holmes and L. Morawska, "A review of dispersion modelling and its application to the dispersion of particles: An overview of different dispersion models available," *Atmospheric Environment*, vol. 40, no. 30, pp. 5902–5928, Sept. 2006.
- [25] J. G. Monroy, J. González-Jiménez, and J. L. Blanco, "Overcoming the Slow Recovery of MOX Gas Sensors through a System Modeling Approach," *Sensors*, vol. 12, no. 10, pp. 13 664–13 680, Oct. 2012.
- [26] J. Monroy, V. Hernandez-Bennetts, H. Fan, A. Lilienthal, and J. González-Jiménez, "GADEN: A 3D Gas Dispersion Simulator for Mobile Robot Olfaction in Realistic Environments," *Sensors*, vol. 17, no. 7, p. 1479, June 2017, number: 7.
- [27] F. Rahbar, A. Marjovi, and A. Martinoli, "An algorithm for odor source localization based on source term estimation," in *IEEE International Conference on Robotics and Automation*, 2019, pp. 973–979.
- [28] W. Jin and A. Martinoli, "Sense in Motion with Belief Clustering: Efficient Gas Source Localization with Mobile Robots," in *2024 IEEE International Conference on Robotics and Automation*, May 2024, pp. 14 909–14 916.
- [29] O. Michel, "Cyberbotics Ltd. Webots™: professional mobile robot simulation," *International Journal of Advanced Robotic Systems*, vol. 1, no. 1, pp. 39–42, 2004.
- [30] "Webots Odor Simulation/Model - Wikibooks, open books for an open world." [Online]. Available: https://en.wikibooks.org/wiki/Webots_Odor_Simulation/Model